A New Rhenanite (β-$NaCaPO_4$) and Hydroxyapatite Biphasic Biomaterial for Skeletal Repair

Sahil Jalota, Sarit B. Bhaduri, A. Cuneyt Tas

School of Materials Science and Engineering, Clemson University, Clemson, South Carolina 29634

Received 9 September 2005; revised 28 October 2005; accepted 10 March 2006
Published online 9 June 2006 in Wiley InterScience (www.interscience.wiley.com). DOI: 10.1002/jbm.b.30598

Abstract: Biphasic β-rhenanite (β-$NaCaPO_4$)–hydroxyapatite ($Ca_{10}(PO_4)_6(OH)_2$) biomaterials were prepared by using a one-pot, solution-based synthesis procedure at the physiological pH of 7.4, followed by low-temperature (300–600°C) calcination in air for 6 h. Calcination was for the sole purpose of crystallization. An aqueous solution of $Ca(NO_3)_2 \cdot 4H_2O$ was rapidly added to a solution of Na_2HPO_4 and $NaHCO_3$, followed by immediate removal of gel-like, poorly-crystallized precursor precipitates from the mother liquors of pH 7.4. Freeze-dried precursors were found to be nanosize with an average particle size of 45 nm and a surface area of 128 m^2/g. Upon calcination in air, precursor powders crystallized into biphasic (60% HA–40% rhenanite) biomaterials, while retaining their submicron particle sizes and high surface areas. β-rhenanite is a high solubility sodium calcium phosphate phase. Samples were characterized by XRD, FTIR, SEM, TEM, ICP-AES, TG, DTA, DSC, and surface area measurements. © 2006 Wiley Periodicals, Inc. J Biomed Mater Res Part B: Appl Biomater 80B: 304–316, 2007

Keywords: bioresorbable; rhenanite; hydroxylapatite; calcium phosphate(s); bone graft

INTRODUCTION

In orthopedic, oral and maxillofacial surgery, a variety of synthetic bone grafts have been used to fill skeletal defects originating from tumor resection, trauma, or infection.[1–3] Synthetic calcium phosphates, such as calcium hydroxyapatite [HA; $Ca_{10}(PO_4)_6(OH)_2$], β-tricalcium phosphate [β-TCP; β-$Ca_3(PO_4)_2$] and biphasic mixtures of these two have found use as bone substitutes.[4–6] HA or β-TCP implants exhibit relatively good tissue compatibility, and new bone is formed directly on the implants with no fibrous encapsulation.[7] However, sintered and well-crystallized HA ceramics usually demonstrated minimal *in vivo* resorption, with resorption times lagging the new bone formation rates.[8–12] Kilian et al.[13] showed that nonsintered HA could even be phagocytized and dissolved by macrophages and osteoclasts, while sintered ceramics were not degraded and remained at the site of implantation for years following the surgery. β-TCP, on the other hand, has a significantly high solubility[14,15] and typically fades away from the defect site even before the completion of new bone formation. An ideal skeletal repair implant should readily take part in the bone remodeling processes, and also allow for the direct anchorage by the bony tissues surrounding it (osteoconduction).[16] If the skeletal repair implant itself causes the *in situ* formation of the mineral part of the bone tissues (osteoinduction) rich in carbonated, apatitic calcium phosphates,[17] while it is continuously resorbing (*in vivo* osseointegration), this could be its most affirmative contribution to the defect site.[18–21] Therefore, efforts in the direction of developing calcium phosphate-based bone substitutes of higher *in vivo* resorbability and osteoinductive/osteoconductive capabilities are still needed.

In stark contrast to sintered HA ceramics,[10,11] calcium phosphate (CaP) self-setting cement formulations, which intentionally employed poorly-crystallized apatite as their major powder component, were shown[22–24] to have significant *in vivo* resorbability (i.e., with resorption rates in excess of 98% in 26 weeks following the implantation in the case of, for instance, α-BSM™, Etex, Cambridge, MA). These cements rapidly took part in the bone remodeling processes by going through phagocytosis under the action of macrophages and osteoclasts.[22] Besides these special orthopedic cements, such high resorption rates with calcium phosphates have only been encountered when the tested (*in vivo*) materials comprised nanoapatites.[25]

Bone is a connective tissue with extracellular substance consisting of a carbonated, apatitic calcium phosphate nanosize mineral dispersed in what is essentially a hydrated collagen matrix. The mineral portion comprises two intimately mixed calcium phosphate phases; (i) noncrystalline or amorphous calcium phosphate and (ii) a poorly-crystallized apatitic calcium phosphate. In the formation of bone mineral, the amorphous phase is laid down first by the bone-depositing cells, i.e., osteoblasts, and subsequently a significant portion

Correspondence to: A. C. Tas, Mersin University, Dept. of Materials Engineering, Mersin 33342, Turkey (e-mail: actas@mersin.edu.tr or actas@clemson.edu)
Contract grant sponsor: NSF; contract grant number: 0522057

of this is then converted in the physiological environment to the carbonated, Na-, K-, and Mg-doped, Ca-deficient bioapatite during the *in vivo* maturation of bones.[26] The presence of the noncrystalline calcium phosphate phase in bones has been detected even by the very first electron microscope studies.[27] The earlier work of Posner and coworkers[28–35] set the foundation for the synthesis and characterization of amorphous or poorly-crystallized calcium phosphate powders. The cytoplasmic calcium phosphate mineral was found to have a structure built up of close-packed ion clusters of about 10 Å similar to those of $Ca_9(PO_4)_6$ present in synthetic amorphous calcium phosphates. Short-range order existed in these amorphous clusters (i.e., Posner clusters) but no long-range order was detected as crystalline hydroxyapatites have.[35] The work of Eanes and coworkers[36–43] and Rey and coworkers[24,44–52] on the preparation of poorly-crystallized calcium phosphates should also be cited in this context.

β-Rhenanite (β-$NaCaPO_4$) is an alkali calcium orthophosphate, which was recently shown to support cellular proliferation together with expression of osteogenic markers at a level higher than β-TCP,[53] and $NaCaPO_4$ was, therefore, suggested to possess a higher potency to enhance osteogenesis than β-TCP. Ramselaar and coworkers[54–57] were the first to investigate the biodegradation rate of $NaCaPO_4$ implants in direct comparison to HA and β-TCP from six weeks to three months *in vivo*. Knabe et al.[58] noted the remarkably high solubility (1.0 g per liter of H_2O at pH 7.[54]) of $NaCaPO_4$ samples in a comparative set of *in vitro* rat bone marrow cell culture tests performed on a number of calcium phosphates. Suchanek et al.[59] discovered the formation of $NaCaPO_4$ interphase layers of high biocompatibility during the hot pressing of hydroxyapatite and bioactive glass powders together. Glass ceramics which contained $NaCaPO_4$ as the crystalline phase were also reported to be bioactive.[60–62]

On the other hand, "Rhenania process" is a well-known procedure mostly used in the fertilizer industry to obtain a soluble phosphate material.[63] In this process, the natural mineral of hydroxyapatite is mixed with Na_2CO_3 and SiO_2 whereas the molar ratio of Na_2CO_3/P_2O_5 fixed at 1.0. SiO_2 is added to prevent the occurrence of free CaO in the sintered product. These powder mixtures are then ground together and calcined in a rotary kiln at about 1000–1200°C for about few hours. Rhenanite, $NaCaPO_4$, of high solubility, has been the major phase in the final product of the Rhenania process.[63] As could be expected, $NaCaPO_4$ received such a high-temperature treatment has a rather low surface area, low surface reactivity, and larger powder particles.

Resorbable, granular bone graft substitutes based on $NaCaPO_4$ formulations have already been commercialized and marketed for the orthopedic surgeons.[64,65] Self-setting cements based on $NaCaPO_4$ are also available for the repair of bone defects.[66] Nevertheless, the powders of such products have been produced by high-temperature (>1100°C) processes.[64]

The motivation for the present study stems from our interest in developing a robust synthesis route for the manufacture of biphasic nanopowders of $NaCaPO_4$ and carbonated, apatitic calcium phosphate using temperatures less than 700°C. Specifically, the apatitic calcium phosphate powders are known to lose their carbonate ions when and if a temperature higher than 700°C was used.[67] The soluble component of these biphasic mixtures (i.e., $NaCaPO_4$), under the *in vivo* action of osteoclasts, is assumed to supply Ca^{2+} ions, as well as hydrogenated phosphate ions, to the surrounding tissues upon implantation. Such materials can, therefore, be expected to act like an osteoinductive stimulant in the body.

Therefore, our experimental approach to that end was framed around the following straightforward supposition: "amorphous or poorly-crystallized calcium phosphate powders are known to consist of nanoparticles of apatitic calcium phosphates,[24] and if those powders were synthesized at the physiological pH in the presence of a rather significant amount of Na^+ ions, then upon calcining those powders over the temperature range of 300–600°C, the resultant material should be a biphasic powder mixture of $NaCaPO_4$ and apatitic calcium phosphate with a high surface area." This work, to the best of the knowledge of authors, reports for the first time the aqueous preparation of nanosize calcium phosphate precursor powders, which are able to readily transform into biphasic powder mixtures of β-$NaCaPO_4$ and carbonated hydroxyapatite upon low-temperature calcination.

MATERIALS AND METHODS

Synthesis of Calcium Phosphate Powder Samples

The synthesis method used to form the Na-containing poorly-crystallized apatitic calcium phosphate powders simply consisted of preparing two solutions, and the procedure adapted here was inspired by the work of Lee et al.[68] Solution-A was prepared as follows; 86.4 g Na_2HPO_4 (disodium hydrogen phosphate, >99%, Fisher Scientific, Fairlawn, NJ) was dissolved in 1.2 L of deionized water, followed by the addition of 60.0 g $NaHCO_3$ (sodium hydrogen carbonate or sodium bicarbonate, >99%, Fisher), which resulted in a clear solution with a pH of about 9 at RT (22±1°C). Solution-B was prepared by dissolving 70.0 g of $Ca(NO_3)_2{\cdot}4H_2O$ (calcium nitrate tetrahydrate, >99%, Fisher) in 500 mL of deionized water. Solution-B was then rapidly added into solution-A under constant stirring (at 250 rpm, with a 5 cm long, Teflon-coated magnetic fish) at room temperature. The pH of the resultant milky suspension (with a nominal Ca/P molar ratio of 0.49) was then rapidly raised to around 7.4, i.e., the physiological pH value, by adding 3–5 mL of concentrated NaOH solution. The solids were immediately filtered by using a filter paper (No. 42, Whatman International, Maidstone, UK) placed in a vacuum-suction porcelain Buechner funnel assembly, and washed with 4 L of deionized water. Upon filtering and washing the precipitates in the funnel one obtains a gel-like calcium phosphate precipitate body (i.e., CaP gel). Some portion of the recovered gels was placed in a glass Petri dish and dried at 37°C for 72 h in static air in a drying oven, while the remainder of the sample was first frozen at −80°C for 2 h, and then lyophilized in a vacuum chamber (Freezone® 4.5, Labconco, Kansas City, MO) kept

at 5×10^{-2} mbar at RT overnight. The above-mentioned synthesis recipe has been repeated six times, and the reproducibility in the composition of precursor powders was checked by consecutive triplicate chemical analyses.

To test the influence of solution pH on the phase composition of the resultant precipitates, in a number of experiments the pH of Solution-A was first decreased to 4.2 at room temperature, under vigorous stirring, by slowly adding aliquots of concentrated HNO_3 (69.2%, Fisher Scientific, Fair Lawn, NJ). The pH value of Solution-B was also reduced to 4.2 by adding HNO_3, followed by adding Solution-B into Solution-A rapidly, as described above. The precipitates were then immediately filtered out of the mother liquor in a fashion similar to that mentioned above.

CaP powders obtained at pH 7.4 placed in clean aluminum oxide crucibles or boats were calcined in a static air atmosphere in an electrically-heated muffle furnace (5°C/min heating and cooling rates) over the temperature range of 300–600°C, with 6 h of soak time at the peak temperatures. Calcined samples were lightly ground (only for few minutes) in an agate mortar by using an agate pestle. To test the sinterability of these rhenanite–HA biphasic samples, we have uniaxially pressed (5000 kg/cm^2) eight pellets (each 1.5 mm thick) out of the 600°C-calcined biphasic powders. These pellets were then separately heated in an electrical resistance, chamber furnace to 1000°C at the rate of 5°C/min, held at that temperature for 6 h, and then cooled back to room temperature within the furnace either at the rate of 5°C/min or 1°C/min.

Powder Characterization

Samples were characterized, at all stages, by powder X-ray diffraction (XRD Model XDS 2000, Scintag, Sunnyvale, CA), scanning electron microscopy (SEM, Model S-4700, Hitachi, Tokyo, Japan), transmission electron microscopy (TEM, Model HD200, Hitachi), Fourier-transform infrared spectroscopy (FTIR, Model Nicolet 550, Thermo-Nicolet, Woburn, MA), inductively-coupled plasma atomic emission spectroscopy (ICP-AES, Model 61E, Thermo Jarrell Ash, Woburn, MA), thermogravimetry (TG/DTA, Model 851e, Mettler-Toledo, Columbus, OH) and differential scanning calorimetry (DSC, Model SDT 2960, TA Instruments, New Castle, DE) analyses, and surface area measurements (Model ASAP 2020, Micromeritics, Norcross, GA).

Powder samples for XRD analyses were first ground in an agate mortar using an agate pestle and then sprinkled onto ethanol-damped single crystal quartz sample holders as a thin and flat layer, followed by tapping to remove the excess of powder. The X-ray diffractometer was operated at 40 kV and 30 mA with monochromated Cu Kα radiation. XRD data were collected in the step mode over the 2θ range of 3°–50°, with a scanning speed corresponding to 0.01° per minute. FTIR samples were first ground in a mortar, in a manner similar to that used in the preparation of XRD samples, and then placed onto the diamond ATR holder of the FTIR spectrometer. This spectrometer was equipped with an Endurance Foundation Series single-bounce diamond ATR (50° incidence angle), and 32 scans were performed at a resolution of 4 cm^{-1}. Powder samples examined with the scanning electron microscope (SEM) were sputter-coated with a thin Pt layer, just prior to imaging, to improve the conductivity of samples. For the transmission electron microscope (TEM) investigations, small aliquots of respective powder samples were first dispersed in pure ethanol, and then few drops of those suspensions were dried on the sample holder grids. The BET surface area of powder samples was determined by applying the standard Brunnauer–Emmet–Teller method to the nitrogen adsorption isotherm obtained at −196°C using the Micromeritics ASAP 2020 instrument. Powder samples used in the ICP-AES analyses were first dissolved in nitric acid prior to measurements. For carbon analyses, 200 mg of powder samples was combusted at around 1200°C in oxygen atmosphere by using a C analyzer (Model Vario Macro, Elementar, Mt. Laurel, NJ). In this process, carbonaceous moieties were converted into CO_2, and after catalytic postoxidation, drying, and cleaning of carrier gas, all carbon oxides are reduced to molecular carbon over a reducing agent and transported by the carrier gas to the thermoconductivity cell for the final quantitative determination of carbon content. Carbon content was then reported by the computer of the instrument as wt % C present in the samples. We converted the measured C contents into CO_3 percentages. Thermogravimetric analyses (TGA) of the CaP gel (or powder) samples were performed in Pt crucibles in a static air atmosphere with a heating rate of 5°C/min from RT to 800°C. Water content of the precursor powders were directly deduced from the TGA traces. DTA and DSC runs were also performed in Pt crucibles in flowing air atmosphere with a heating rate of 5°C/min, and Al_2O_3 powder was used as the reference sample in these experiments.

RESULTS AND DISCUSSION

The synthesis procedure described in *Synthesis of Calcium Phosphate Powder Samples* was able to produce apatitic calcium phosphate powders when the synthesis solution pH was maintained at 7.4. The results and data given below are all for pH 7.4 samples, unless otherwise noted. XRD data for 37°C- and freeze-dried CaP gels were given in the comparative chart of Figure 1(a). Both traces were characteristic of poorly-crystallized CaP powders,[24,46–52] although drying at 37°C seemed to cause a slight increase in the overall crystallinity with respect to freeze drying. In freeze drying, the water initially present was gradually sublimed, whereas in 37°C drying that water present at the end of the washing step helped the crystallization to proceed at a low rate. Freeze-dried powders were found to be fluffier with respect to those dried at 37°C, therefore, after the preliminary experiments all of the powders obtained by aqueous synthesis procedure were freeze-dried. Surface area measurements also confirmed this observation, and the BET surface area of freeze-dried powders was 128 ± 5, whereas that of the powders dried at 37°C for 72 h was 62 ± 3 m^2/g.

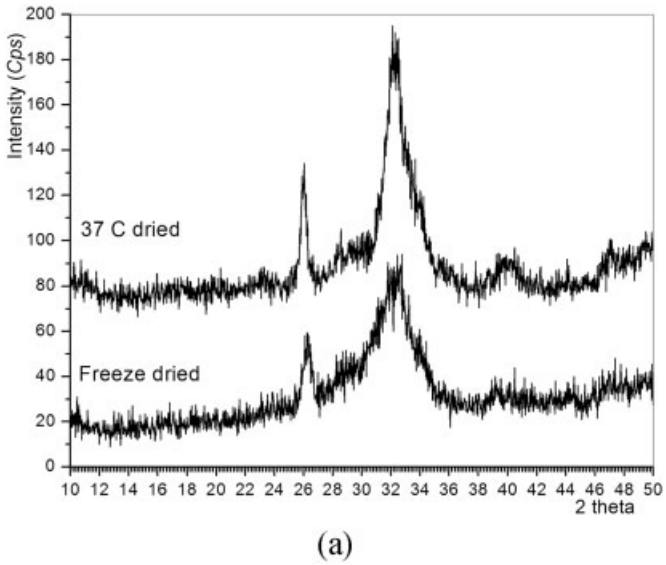

Figure 1. (a) XRD traces of 37°C-heated and freeze-dried CaP gel precursors

Adult human bones yield XRD data very similar to those given in Figure 1(a).[69,70] If the syntheses were to be carried out under refrigeration, e.g., at around 4°C, the XRD charts obtained would consist of, more or less, X-ray amorphous traces.[68] The hydrated nature of CaP gel samples dried at 37°C were also confirmed by the wide water bands displayed in their FTIR spectra given in Figure 1(b). On the other hand, in the FTIR spectra of freeze-dried samples, the intensities of those water bands have been significantly reduced [Figure 1(b)]. Therefore, drying at 37°C did not completely eliminate the water present in those precipitated precursor gels. The symmetric and antisymmetric stretching of the PO_4^{3-} group were observed at 1097, 1043, 964, 604, and 565 cm^{-1}. Bands of CO_3^{2-} ions were observed at 1470–1420 and 875 cm^{-1}.

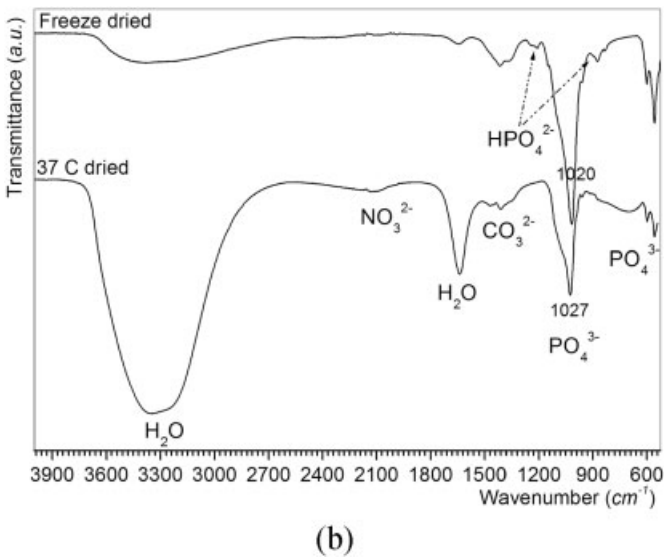

Figure 1. (b) FTIR traces of 37°C-heated and freeze-dried CaP gel precursors

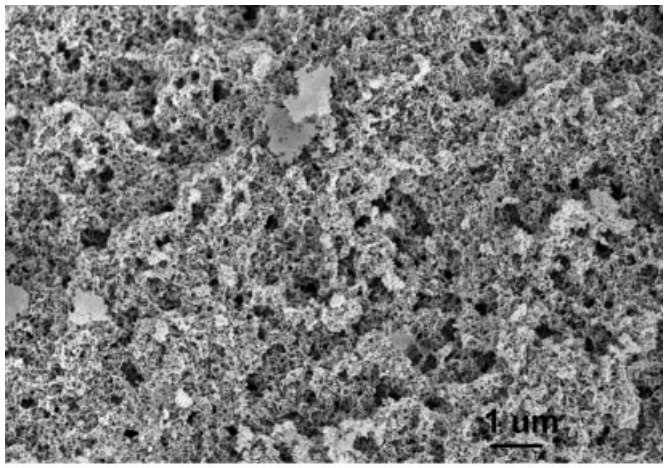

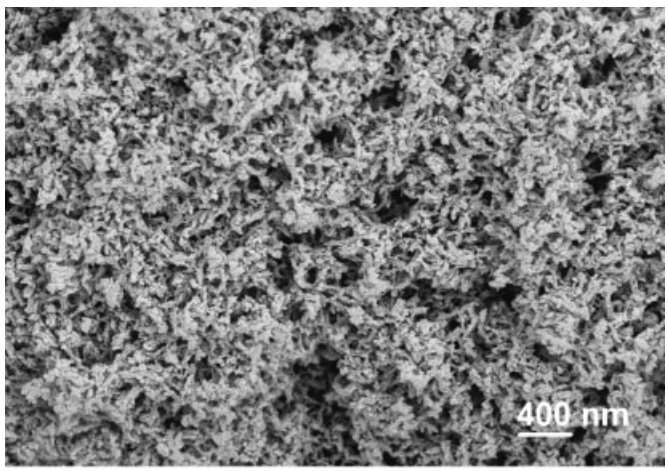

Figures 1. (c) & (d) SEM micrographs of freeze-dried CaP gel precursors at two different magnifications

The very weak IR band at around 919 cm^{-1} and again the weak shoulder at around 1297–1310 cm^{-1} were attributed to the smaller presence of HPO_4^{2-} ions.[71] HPO_4^{2-} ions do also have a band at 874 cm^{-1}, which partially overlaps with that of CO_3^{2-} ions rendering the distinction between HPO_4^{2-} and CO_3^{2-} ions more difficult. In contrast to our findings, Wu et al.[45] previously noted that unique HPO_4^{2-} group present in the human bone mineral was not seen in synthetic CaP samples produced under conditions similar to those of this study. The synthesis procedure adopted and used in this study was, therefore, able to produce a hydrated and carbonated CaP gel precursors, which contained a trace amount of protonated orthophosphate ions similar to the human fetal bones [Figure 1(b)].

The ICP-AES and C analyses results are given in Table I. Analyses were performed in triplicate on all the samples. Freeze-dried CaP gel precursors gave the following medians: Ca: 21.27 ± 0.02%; P: 13.27 ± 0.01% and Na: 9.10 ± 0.01 wt %, which corresponded to a molar Ca/P ratio of 1.239 (Table I), and a molar (Na+Ca)/P ratio of 2.163 in these

TABLE I. Results of ICP-AES and C Analyses (in wt %, average of 3 runs)

	Sample					
	Ca	P	Ca/P (molar)	Na	C	CO_3
Freeze-dried	21.27	13.27	1.239	9.10	0.82	4.10
300°C	28.93	17.99	1.243	8.98	0.58	2.90
400°C	28.49	18.06	1.219	9.02	0.39	1.95
500°C	28.36	17.88	1.226	9.35	0.32	1.60
600°C	29.17	18.30	1.232	9.16	0.21	1.05
1000°C	28.64	18.04	1.227	9.09	0.01	0.05

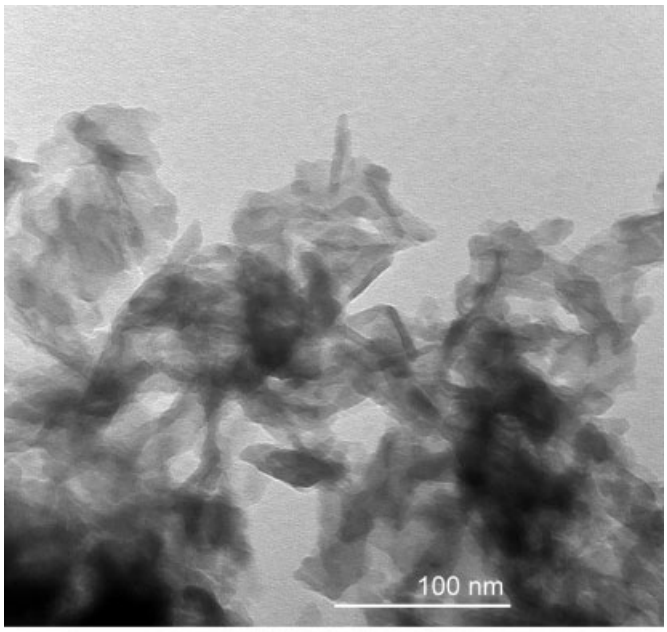

Figures 2. (a) & (b). TEM micrographs of freeze-dried CaP gel precursors.

powders. It is not so surprising that even if one started with a nominal precipitation solution Ca/P molar ratio of around 0.5, the precipitates formed at or near the physiological pH would still be Ca-deficient apatitic CaP. C analyses proved that the precursor powders were carbonated, and the carbonate content decreased with an increase in the calcination temperature, while the Ca/P molar ratio and the Na content remained almost the same.

When the pH values of the same precipitation solutions were fixed at around 4.2, then the formed powders only consisted of the brushite phase (DCPD, $CaHPO_4 \cdot 2H_2O$), whose XRD and FTIR data are not shown here to save space. The size and shape of those brushite crystals were also perfectly the same as mentioned elsewhere.[72]

The SEM morphology of the freeze-dried powders was shown, at two different magnifications, in Figures 1(c) and 1(d). The bright-field TEM photomicrographs given in Figures 2(a) and 2(b) depicted the nanostructure of the same powders. It should be noted that the selected-area electron diffraction inset of Figure 2(b) proved the nanocrystalline nature of those powders. TG/DTA/DSC analyses of the freeze-dried CaP precursors [Figure 2(c)] indicated that upon

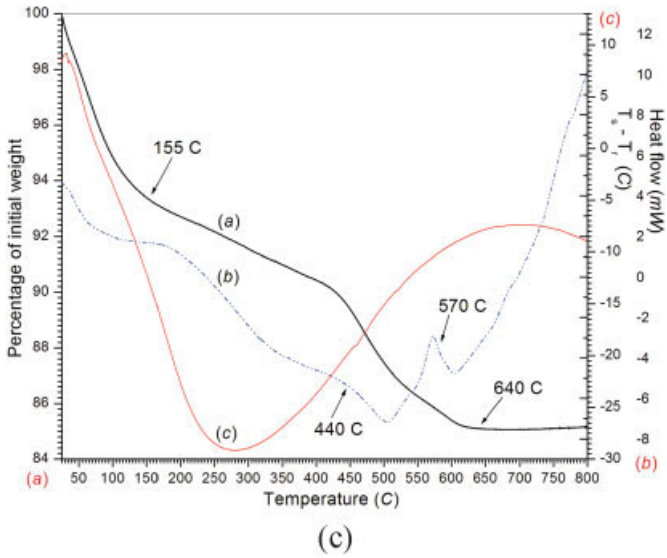

(c)

Figure 2. (c) TG/DTA/DSC spectra of freeze-dried CaP gel precursors; (a) TG, (b) DSC, and (c) DTA spectra. [Color figure can be viewed in the online issue, which is available at www.interscience.wiley.com.]

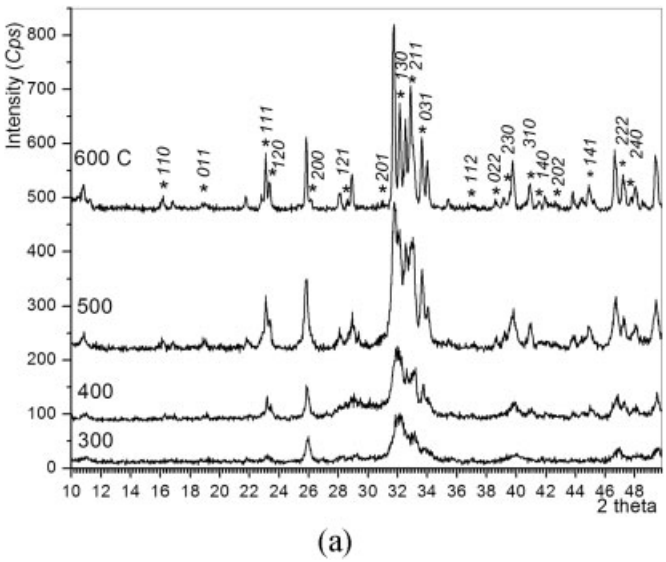

Figure 3. (a) XRD spectra of CaP gel precursors heated in air from 300°C to 600°C (* and the respective *hkl* indices denote the reflections of β-NaCaPO$_4$, all the other peaks belong to HA)

heating to 155–160°C the samples first lost around 7.5% of their initial weight. This corresponded to the adsorbed water. Therefore, the water content of the precursor powders was deduced to be around 7 to 7.5%. With continued heating to 415°C, another gradual weight loss of about 2.5% was observed, and this was probably due to the volatilization of the remnants of nitrate ions. Characteristic IR bands for nitrate ions were to be found at 1440–1300 and 1070–1030 cm^{-1},[73] but in the IR spectra of Figure 1(b) it was quite difficult to identify those nitrate bands because of severe overlapping with the phosphate and carbonate bands over the same range. However, the weak bands at around 2200–2030 cm^{-1} in Figure 1(b) can be ascribed to the nitrates.[74] Further heating at above 415°C, up to 650°C, displayed the removal of carbonate ions that was accompanied with a weight decrease of around 5 wt %, bringing up the total weight loss to 15%. The temperature when one reached constant weight was 640°C [Figure 2(c)].

β-Rhenanite, i.e., β-NaCaPO$_4$, phase in these gel precursors started to crystallize upon low-temperature calcination of the samples over the temperature range of 300–600°C. Especially, the DSC spectrum given in Figure 2(c) showed that there were two exothermic events taking place over the temperature range of 440–570°C. The starting points of these exothermic events were indicated with arrows in Figure 2(c). It should be noted that DSC is a dynamic process taking place at a heating rate of 5°C/min, and under isothermal heatings the starting points of those exothermic events would be slightly lower than those indicated by the TG/DTA/DSC spectra. XRD spectra of Figure 3((a) showed the crystallization of NaCaPO$_4$ in a matrix of apatitic calcium phosphate. β-NaCaPO$_4$ (sometimes it may also be written as CaNaPO$_4$) has an orthorhombic (space group Pnam[62]) unit cell with the lattice parameters of $a = 6.797$, $b = 9.165$, and $c = 5.406$ Å.[75] This phase (which will transform into α-NaCaPO$_4$ at 650°C) is also isostructural with β-K$_2$SO$_4$. The most straightforward way of synthesizing phase-pure NaCaPO$_4$ powders can be the solid state reactive firing of the powder mixtures (in a 1:2:2 molar ratio) of Na$_2$CO$_3$, CaCO$_3$, and (NH$_4$)$_2$HPO$_4$ at 900–950°C.[75] However, such a synthesis route (which involves the formation of liquid phases upon melting of first (NH$_4$)$_2$HPO$_4$ and then Na$_2$CO$_3$) will not be able to yield nanosize, therefore, high surface area and high surface reactivity powders.[76] The peaks denoted by * (and their respective *hkl* reflections) were those of β-NaCaPO$_4$, and the 2θ positions of such peaks were in close agreement with those given in ICDD PDF 29–1193. Upon heating at 600°C, CaP gel precursors of this study crystallized about 40±3% β-NaCaPO$_4$. This value was calculated from the data of Figure 3(a) by using the relative intensity ratio of the most intense peak of hydroxyapatite (at 31.78° 2θ) to that of NaCaPO$_4$ (at 32.59° 2θ). The samples heated at 600°C for 6 h can therefore be named as 40% NaCaPO$_4$–60% HA biphasic biomaterials.

FTIR traces of the same calcined samples were depicted in Figure 3(b). CaP precursors calcined even at the low temperature of 300°C were able to exhibit the characteristic OH$^-$ stretching vibration at 3572 cm^{-1}, and this band became more pronounced with the increase in calcination temperature at or above 500°C. The OH$^-$ bending vibration was also recorded at 634 cm^{-1}.[77] These bands proved that the freeze-dried apatitic calcium phosphate phase (which lacked the OH vibrations) present in the gel precursors completely converted into hydroxyapatite upon calcination. Precipitated apatitic calcium phosphate precursors need the humidity in the calcination atmosphere to transform into Ca–hydroxyapatite upon heating.[78–82] The relative humidity in our laboratories was at around 65–70% during those calcination runs. Characteristic FTIR spectrum of pure β-NaCaPO$_4$ was previously given by Driessens et al.[55] The orthophosphate stretching

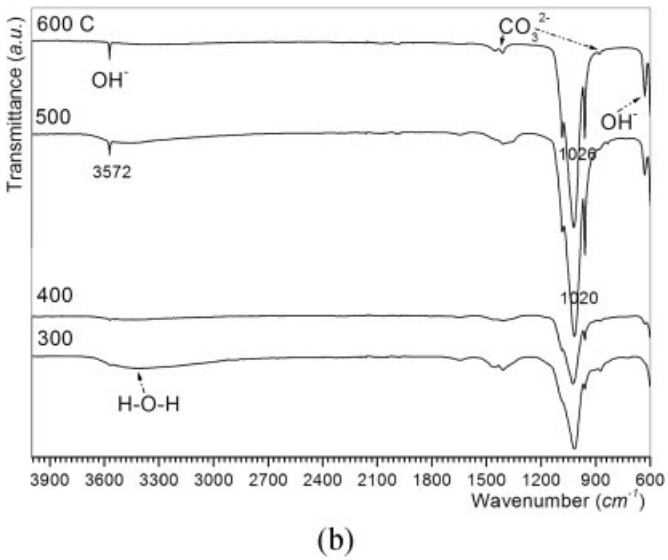

Figure 3. (b) FTIR traces of CaP gel precursors heated in air for 6 h from 300°C to 600°C

bands for the 500°C-calcined samples were observed at 603 (ν_4), 962 (ν_1), 1020, and 1089 (ν_3) cm^{-1}, which were contributed both by crystalline β-rhenanite and apatitic calcium phosphate.[77] The absence of the P—O—P vibrational mode of pyrophosphates at 740 cm^{-1} [Figure 3(b)] proved that the calcined samples did not contain any traces of $Ca_2P_2O_7$.[77] If the amount of HPO_4^{2-} ions in the precursor powders were significant, then their conversion into pyrophosphate would have been inevitable through the reaction $2HPO_4^{2-} \rightarrow P_2O_7^{4-} + H_2O$, which takes place at 600°C.[31] Moreover, Loong et al.[83] definitively demonstrated the lack or significant deficiency of OH^- ions occupying crystallographic sites in the Ca-deficient, nonstoichiometric apatitic crystals of rat and bovine bones by using inelastic neutron-scattering spectroscopy.

It is known that an IR band at 1020 cm^{-1} can be attributed to the ν_3 vibration of PO_4^{3-} in nonstoichiometric or Ca-deficient and/or carbonated apatitic calcium phosphates; however, a band recorded at 1030 cm^{-1} is pinpointing to the ν_3 vibration of PO_4^{3-} in stoichiometric hydroxyapatite.[84] Therefore, the relative ratios of 1020/1030 bands in the FTIR spectra could provide a measure of mineral crystallinity and maturity in bone minerals or apatitic-looking calcium phosphates.[77,85] While the samples calcined at 300°C or 500°C were displaying that orthophosphate ν_3 vibration at 1020 cm^{-1}, the same vibration was found to shift to 1026 cm^{-1} in the 600°C-calcined sample [see Figure 3(b)]. This can be ascribed to the transition from nonstoichiometric to stoichiometric apatite together with the crystallization of β-$NaCaPO_4$ phase. On the other hand, it is interesting to note here that for the gel precursor samples dried at 37°C the same ν_3 vibration was recorded at 1027 cm^{-1}, whereas the freeze-dried samples had it at 1020 cm^{-1}, as shown in the IR traces of Figure 1(b). This means that drying those gel precursors at 37°C for 72 h may have a positive effect on the progress of crystallization or so-called "maturation."

Variations in the grain size and morphology of the rhenanite-hydroxyapatite biphasic powders, as a function of increasing calcination temperature, were monitored by the SEM photomicrographs given in Figure 4. The cracked-like grain/particle surfaces seen especially in the high magnification micrographs of Figure 4 are the artifacts created by the Pt-coating layer. Grain sizes directly measured from the SEM micrographs, as well as the respective surface areas of these powders, is given in Table II.

Even after light calcination at temperatures from 300 to 600°C, these materials retained their initially small grain sizes still in the nano- or submicron-range. These surface area data were quite comparable to those reported by Somrani et al.[51] in a study on the thermal evolution of poorly-crystalline apatitic calcium phosphate powders produced by using Ca-nitrate tetrahydrate and diammonium hydrogen phosphate as the starting water soluble reagents, in the absence of any Na ions in their precipitation solutions. Apatitic calcium phosphate samples of Somrani et al.[51] decomposed into crystalline tricalcium phosphate upon calcination. Freeze-dried samples of the current study consisted of (as shown in the micrographs

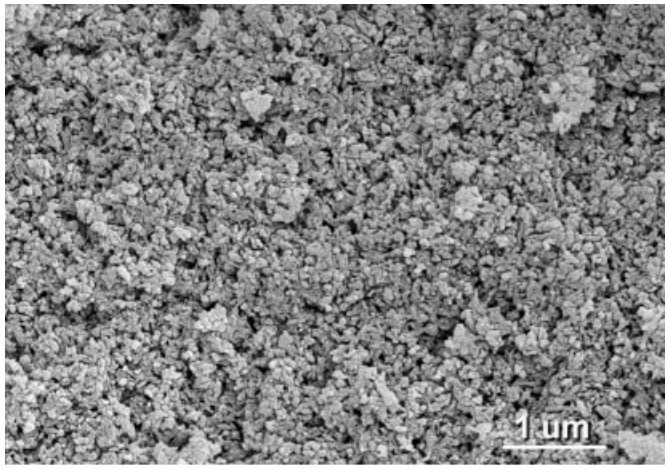

(a)

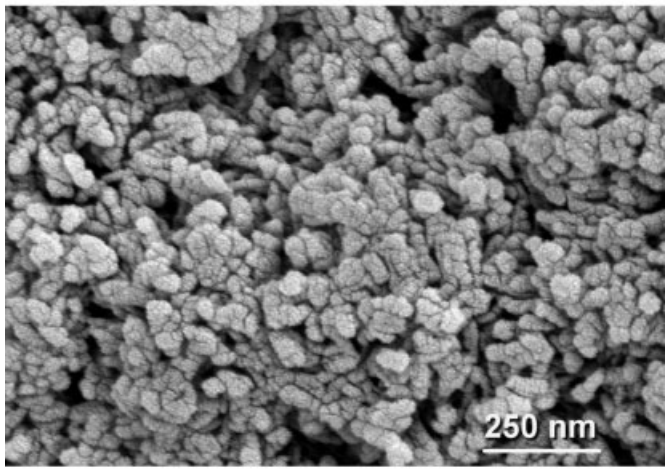

(b)

Figures 4. (a) & (b) SEM morphology of freeze-dried CaP gel precursors heated at 300°C at two different magnifications

of Figures 1 and 2) particles (or moieties) having a needlelike morphology with average dimensions of 10 (thickness) and 70 (length) nanometer. These are very well within the size range of bone apatite crystals, which were documented by using electron microscopy for more than 5 decades ago.[27,86] Johansen and Parks[87] reported that bone apatite crystallites were platelike in shape with dimensions 400 × 200–350 × 25–50 Å. Upon calcination of the samples of this study, those initially plate- or needle-like, longitudinal moeities present in the freeze-dried powders (Figures 1 and 2) tended to form more or less equiaxed or globular grains (Figure 4). Such a tendency of nanosize globule formation upon heating can also be taken as a sign of those moieties (Figure 2) actually being comprised of very much smaller particles. Indeed, early studies by Molnar[88,89] suggested that bone crystals are composed of chains of microcrystals fused in an end-to-end relationship. An X-ray diffraction study by Posner et al.[90] reported that the largest dimension of the bone apatite crystals was about 100 Å, and those apatitic crystallites should be regarded as a mosaic of microcrystals rather than as a continuously uni-

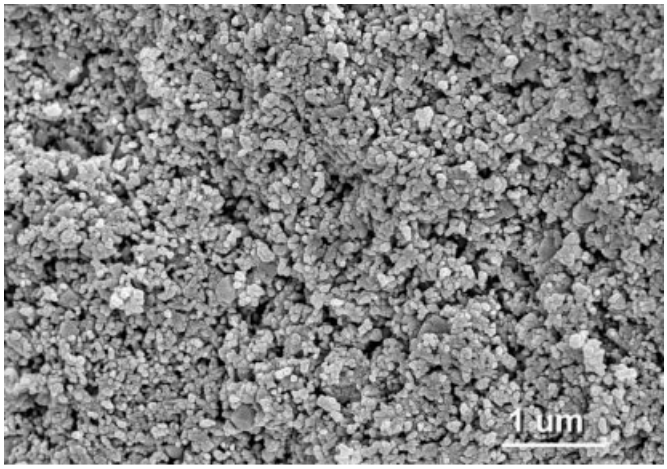

(c)

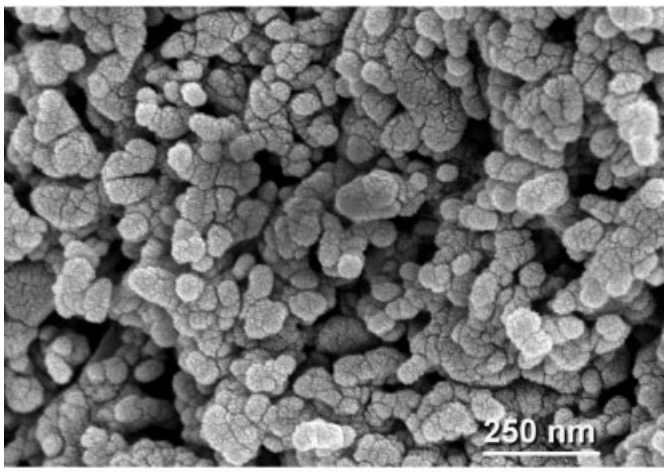

(d)

Figures 4. (c) & (d) SEM morphology of freeze-dried CaP gel precursors heated at 400°C at two different magnifications

form, single crystal.[31] The sodium-doped calcium phosphate gel precursors of this study [enthused by the work of Refs. 24, 48, 68] consisted of poorly-crystallized apatitic microcrystals very similar in dimensions and appearance to those of bone mineral.

Nakahira et al.,[91] in a study of testing the applied magnetic field on the bioactivity of hydroxyapatite, reported the formation of $NaCaPO_4$ as a second phase in 10% $NaHCO_3$-mixed hydroxyapatite bioceramic samples upon sintering those at 1000°C. These authors blended the hydroxyapatite and $NaHCO_3$ (at 10% level) powders by using a conventional ball-mill, followed by compaction, cold isostatic pressing, and sintering. Nakahira et al.[91] also tested the bioactivity of those 1000°C-sintered samples by soaking them, at 37°C, in SBF (simulated/synthetic body fluid[92,93]) solutions from 4 to 7 days. It is quite interesting to note here that, under the identical SBF soaking conditions, according to Nakahira et al.,[91] while the pure hydroxyapatite samples (with no magnetic field application) were not showing any bonelike CaP deposits on their surfaces, $NaCaPO_4$-containing samples were covered with a high abundance of such deposits. This was again attributed to the higher bioactivity of $NaCaPO_4$ phase than that of pure hydroxyapatite.[91,94] Although we did not include an SBF-soaking study in this manuscript, the strong evidence brought upon by the work of Nakahira et al.[91] was considered to be sufficient to ascertain the bioactivity (in SBF solutions) of such $NaCaPO_4$-containing hydroxyapatite bioceramics. Moreover, the presence of Na ions that weaken the bond between Ca^{2+} and PO_4^{3-} in the crystal surface accounts for the high dissolution rate of β-$NaCaPO_4$. If the surface of a bioceramic sample inserted in an SBF solution exhibits such a significant ionic level dissolution phenomenon, then the Ca^{2+} and HPO_4^{2-} ions to be abundant on these surfaces will further trigger the aggregation, and the consequent surface segregation, of Posner's clusters found in those solutions.[95]

The $NaCaPO_4$–HA biphasic powders of this study sintered well even after heating them at the low temperature of 1000°C for 6 h in air as pressed pellets. The SEM photomicrographs given in Figures 5(a) and 5(b) (insets showed a

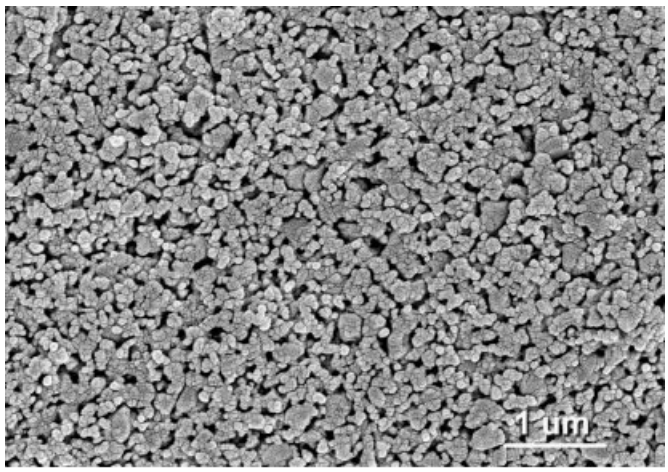

(e)

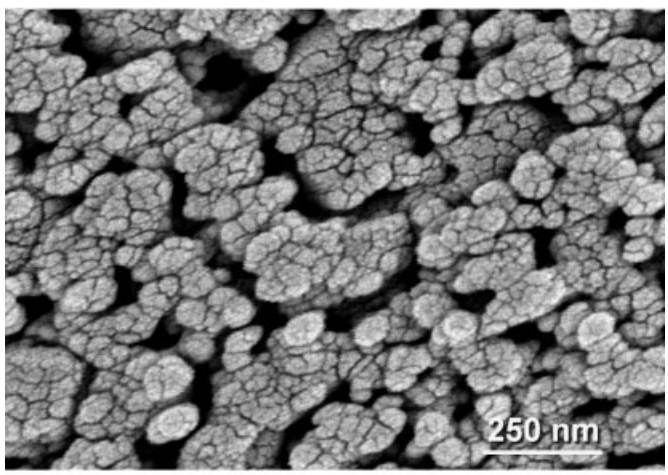

(f)

Figures 4. (e) & (f) SEM morphology of freeze-dried CaP gel precursors heated at 500°C at two different magnifications

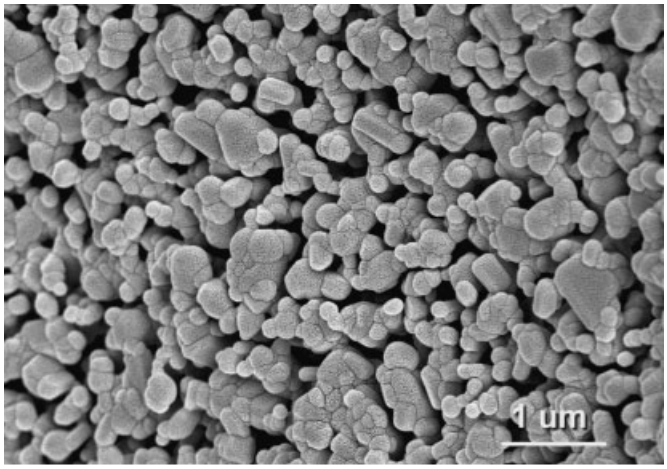

(g)

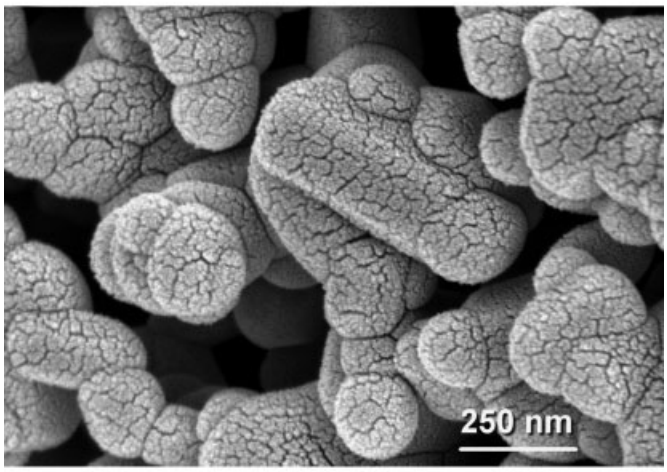

(h)

Figures 4. (g) & (h) SEM morphology of freeze-dried CaP gel precursors heated at 600°C at two different magnifications

higher magnification view) depicted the surface of the well-densified pellets heated at 1000°C for 6 hours after cooling at the rate of 5°C/min and 1°C/min, respectively. It is interesting to note that even the chemically synthesized, submicron HA-TCP biphasic powders do not show a densification rate (even after heating those at 1200°C) as high as the samples of this study.[96] Cooling rate was found to have a pronounced effect on the $NaCaPO_4$–HA biphasic samples though. Samples cooled at the rate of 5°C/min [Figure 5((a)] showed a larger number of both inter- and intra-granular cracks, when

TABLE II. Grain Sizes and Surface Areas of Powders

Sample	Grain size (nm)	Surface area (m^2/g)
Freeze-dried	45 ± 10	128 ± 5
300°C	60 ± 10	79 ± 4
400°C	100 ± 10	70 ± 5
500°C	150 ± 20	53 ± 3
600°C	300 ± 70	34 ± 3

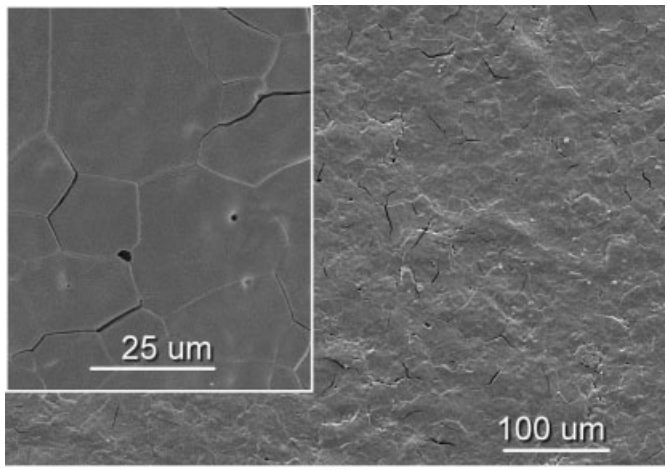

(a)

Figure 5. (a) 600°C-calcined biphasic powders sintered at 1000°C for 6 h and cooled at the rate of 5°C/min

the cooling rate was decreased to 1°C/min [Figure 5(b)] those cracks were reduced. The mismatch between the coefficients of thermal expansion of $NaCaPO_4$ and HA phases might be responsible for the formation of those cracks. Pellets sintered at 1000°C still had the same biphasic nature (i.e., 60% HA–40% $NaCaPO_4$) and their XRD spectra were in strong resemblance to those given in Figure 3(a) for the 600°C-calcined powder sample. Sintering the biphasic samples at 1000°C for 6 hours did not destroy the original phase constitution. However, as expected, the FTIR spectra of the 1000°C-sintered pellets did not exhibit the carbonate bands. Carbonate ions in apatitic calcium phosphate structures cannot easily persist at temperatures greater than 700–750°C. Nevertheless, a more detailed study of the sintering behavior of these biphasic powders, with the aim of forming dense, carbonate ion-free ceramics of low surface area, over the temperature range of >1000–1300°C was out of the scope of this study.

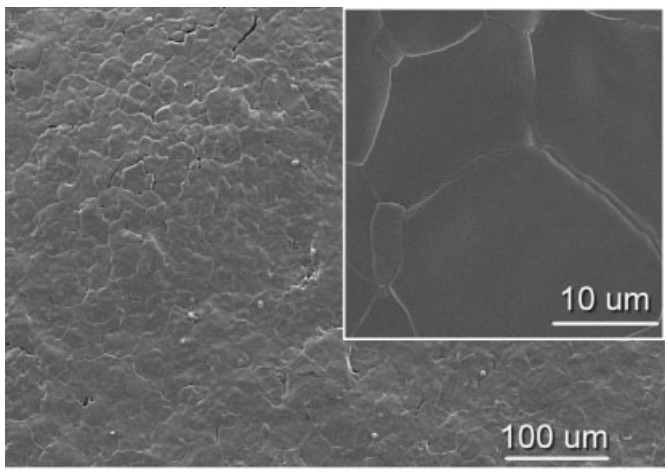

(b)

Figure 5. (b) 600°C-calcined biphasic powders sintered at 1000°C for 6 h and cooled at the rate of 1°C/min

β-$NaCaPO_4$ phase was recently reported by El-Ghannam[61] to form upon the calcination (180–800°C) of a new class of SiO_2–$CaHPO_4 \cdot 2H_2O$ physically-mixed powder blends initially wetted by rather concentrated NaOH solutions. *In vivo* studies performed by El-Ghannam[61] found that these materials were superior to Bioglass® in terms of protein absorption, enhancement of bone generation, and overall resorption. Gong et al.[60] reported that crystalline β-rhenanite in contact with SBF solutions may act as a nucleation precursor for the formation of apatitic calcium phosphates with respect to the following reaction:

$$3NaCaPO_4 + 2Ca^{2+} + H_2O \rightarrow Ca_5(PO_4)_3OH + 3Na^+ + H^+. \quad (1)$$

Kangasniemi et al.[97] prepared β-rhenanite powders by sintering stoichiometric mixtures of $CaHPO_4$ and Na_2CO_3 at 1300°C, followed by sieving the ground sintered chunks to a size below 45 μm, and used those later as crystalline additives (from 20 to 30 wt %) in their experimental bioactive glass compositions. The same authors were then reported in a separate study[98] the dissolution behavior of crystalline β-rhenanite- or crystalline HA-containing bioactive glasses soaked in SBF from 5 h to 6 days. Kangasniemi et al.[98] concluded that the β-rhenanite-containing composites had a very positive effect on the rate of apatitic CaP layer formation on the surfaces of samples soaked in SBF.

The earlier but quite comprehensive work of Ramselaar et al.[54–56] should be taken as a good reference for the strong potential of β-rhenanite in developing resorbable or osteoinductive calcium phosphate bioceramics. The *in vivo* canine studies performed by Ramselaar et al.[56] demonstrated that statistically more bone deposition occurred on β-rhenanite particles than on hydroxyapatite particles.

This study showed that by simple calcination of a poorly-crystallized, Na-containing calcium phosphate gel precursor synthesized at the physiological pH it will be possible to form biphasic biomaterials consisting of a high solubility β-$NaCaPO_4$ and less soluble nanosize hydroxyapatite. Since the starting material is a gel precursor, it can be easily shaped (for instance, by extrusion, injection molding or solid freeform fabrication techniques) into any desired three-dimensional form before the full crystallization of the phases to take place during the final calcination step. The initial viscosity of such gels can be readily adjusted prior to the form fabrication. We have also observed that these gels can even be stored in ordinary zip-lock, air-tight nylon bags for more than a year (under refrigeration at 4°C), without resulting in any detectable changes in their XRD and FTIR patterns. Moreover, leachable porogen phases or particulates (such as, NaCl, ammonium carbonate, ammonium acetate, ice crystals, etc.) may also be incorporated into these gels for forming porous bodies at the end of the fabrication processes. The only delicate step in the use of such preformed gels for forming 3D shapes would be the careful drying in a relative humidity-controlled environment that should avoid the formation of drying cracks due to the rapid removal of entrapped water.

The osteoinductive character reported[99–101] for the biphasic β-TCP (40%) and HA (60%) biomaterials may also be expected for the β-rhenanite-HA materials of this study. Finally, to validate the above speculation and the clinical usefulness of the β-rhenanite + HA biphasic biomaterials of this work *in vivo* studies must be performed, which we plan to report in a follow-up study.

CONCLUSIONS

Sodium-doped calcium phosphate precursors were produced at room temperature by using a robust aqueous synthesis procedure involving the use of Na_2HPO_4, $NaHCO_3$, and $Ca(NO_3)_2 \cdot 4H_2O$. The precursors formed at the physiological pH of 7.4 were in the form of a gel. Upon freeze-drying, these precursor gels were found to consist of poorly-crystallized, nanosize apatitic calcium phosphates with a surface area in excess of 120 m^2/g. Calcination of these samples in a static air atmosphere over the temperature range of 400–600°C for 6 h led to the production of β-rhenanite and hydroxyapatite biphasic biomaterials. Calcined powder samples had surface areas over the range 30 to 80 m^2/g, and consisted of nanosize grains.

Authors gratefully acknowledge the hands-on participation of the high school student Rosie M. Knotts, as a laboratory assistant for two weeks, at the very start of this research project in June 2004.

REFERENCES

1. Schmitz JP, Hollinger JO. The critical size defect as an experimental model for craniomandibulofacial nonunions. Clin Orthop 1986;205:299–308.
2. Yaszemski MJ, Payne RG, Hayes WC, Langer R, Mikos AC. Evolution of bone transplantation: Molecular, cellular and tissue strategies to engineer human bone. Biomaterials 1996; 17:175–185.
3. Jarcho M. Calcium phosphate ceramics as hard tissue prosthetics. Clin Orthop 1981;157:259–278.
4. Nunes CR, Simske SJ, Sachdeva R, Wolford LM. Long-term ingrowth and apposition of porous hydroxylapatite implants. J Biomed Mater Res 1997;36:560–563.
5. Nicholas RW, Lange TA. Granular tricalcium phosphate grafting of cavitary lesions in human bone. Clin Orthop 1994;306: 197–203.
6. Elliott JC. Structure and Chemistry of the Apatites and Other Calcium Orthophosphates. Amsterdam: Elsevier; 1994.
7. Spector M. Anorganic bovine bone and ceramic analogs of bone mineral as implants to facilitate bone regeneration. Clin Plast Surg 1994;21:437–444.
8. Metsger DS, Driskell TD, Paulsrud JR. Tricalcium phosphate ceramic—A resorbable bone implant: Review and current status. J Am Dent Assoc 1982;105:1035–1038.
9. Schmitz JP, Hollinger JO, Milam SB. Reconstruction of bone using calcium phosphate bone cements: A critical review. J Oral Maxillofac Surg 1999;57:1122–1126.
10. Joschek S, Nies B, Krotz R, Goepferich A. Chemical and physicochemical characterization of porous hydroxyapatite ceramics made of natural bone. Biomaterials 2000;21:1645–1658.

11. Hing KA, Best SM, Tanner KE, Bonfield W, Revell PA. Mediation of bone ingrowth in porous hydroxyapatite bone graft substitutes. J Biomed Mater Res A 2004;68:187–200.
12. Kamakura S, Sasano Y, Shimizu T, Hatori K, Suzuki O, Kagayama M, Motegi K. Implanted octacalcium phosphate is more resorbable than β-tricalcium phosphate and hydroxyapatite. J Biomed Mater Res 2002;59:29–34.
13. Kilian O, Wenisch S, Heiss C, Horas U, Dingeldein E, Schnettler R. Einfluss von Ostim kombiniert mit autologen thrombozytaeren Wachstumsfaktoren. Biomaterialien 2002;3:126–132.
14. Tang R, Hass M, Wu W, Gulde S, Nancollas GH. Constant composition dissolution of mixed phases. II. Selective dissolution of calcium phosphates. J Colloid Interface Sci 2003;260:379–384.
15. Kwon SH, Jun YK, Hong SH, Kim HE. Synthesis and dissolution behavior of β-TCP and HA/β-TCP composite powders. J Eur Ceram Soc 2003;23:1039–1045.
16. Hoshikawa A, Fukui N, Fukuda A, Sawamura T, Hattori M, Nakamura K, Oda H. Quantitative analysis of the resorption and osteoconduction process of a calcium phosphate cement and its mechanical effect for screw fixation. Biomaterials 2003;24:4967–4975.
17. Yuan HP, Yang ZJ, Li YB, Zhang XD, De Bruijn JD, De Groot K. Osteoinduction by calcium phosphate biomaterials. J Mater Sci: Mater Med 1998;9:723–726.
18. Goyenvalle E, Guyen NJM, Aguado E, Passuti N, Daculsi G. Bilayered calcium phosphate coating to promote osseointegration of a femoral stem prosthesis. J Mater Sci: Mater Med 2003;14:219–227.
19. Szpalski M, Gunzburg R. Applications of calcium phosphate-based cancellous bone void fillers in trauma surgery. Orthopedics 2002;25:S601–S609.
20. Neuman WF, Neuman MW. The Chemical Dynamics of Bone Mineral. Chicago: Chicago University Press; 1958.
21. Tas AC. Participation of calcium phosphate bone substitutes in the bone remodeling process: Influence of materials chemistry and porosity. Key Eng Mater 2004;264–268:1969–1972.
22. Wenisch S, Stahl JP, Horas U, Heiss C, Kilian O, Trinkaus K, Hild A, Schnettler R. In vivo mechanisms of hydroxyapatite ceramic degradation by osteoclasts: Fine structural microscopy. J Biomed Mater Res A 2003;67:713–718.
23. Bloemers FW, Blockhuis TJ, Patka P, Bakker FC, Wippermann BW, Haarman HJTM. Autologous bone versus calcium–phosphate ceramics in treatment of experimental bone defects. J Biomed Mater Res B 2003;66:526–531.
24. Knaack D, Goad MEP, Aiolova M, Rey C, Tofighi A, Chakravarthy P, Lee DD. Resorbable calcium phosphate bone substitute. J Biomed Mater Res 1998;43:399–409.
25. Muller-Mai CM, Stupp SI, Voigt C, Gross U. Nanoapatite and organoapatite implants in bone: Histology and ultrastructure of the interface. J Biomed Mater Res 1995;29:9–18.
26. Eanes ED, Termine JD, Posner AS. Amorphous calcium phosphate in skeletal tissues. Clin Orthop Relat Res 1967;53:223–235.
27. Robinson RA, Watson ML. Collagen–crystal relationships in bone as seen in the electron microscope. III. Crystals and collagen morphology as a function of age. Ann N Y Acad Sci 1955;60:596–628.
28. Posner AS, Stephenson SR. Crystallographic investigation of tricalcium phosphate hydrate. J Dent Res 1952;31:371–382.
29. Stutman JM, Lippincott ER, Posner AS. Hydrogen bonding in the calcium phosphates. Nature 1962;193:368–370.
30. Termine JD, Posner AS. Amorphous/crystalline interrelationships in bone mineral. Calcif Tissue Res 1967;1:8–23.
31. Posner AS. Crystal chemistry of bone mineral. Physiol Rev 1969;49:760–792.
32. Blumenthal NC, Holmes JM, Posner AS. Effect of preparation conditions on the properties and transformation of amorphous calcium phosphate. Mater Res Bull 1972;7:1181–1190.
33. Boskey AL, Posner AS. Magnesium stabilization of amorphous calcium phosphate: A kinetic study. Mater Res Bull 1974;9:907–916.
34. Blumenthal NC, Betts F, Posner AS. Effect of carbonate and biological macromolecules on formation and properties of hydroxyapatite. Calcif Tissue Res 1975;18:81–90.
35. Betts F, Blumenthal NC, Posner AS, Becker GL, Lehninger AL. Atomic structure of intracellular amorphous calcium phosphate deposits. Proc Natl Acad Sci USA 1975;72:2088–2090.
36. Nylen U, Eanes ED, Termine JD. Molecular and ultrastructural studies of noncrystalline calcium phosphates. Calcif Tissue Res 1972;9:95–108.
37. Greenfield DJ, Eanes ED. Formation chemistry of amorphous calcium phosphates from carbonate-containing solutions. Calcif Tissue Res 1972;9:152–162.
38. Termine JD, Eanes ED. Comparative chemistry of amorphous and apatitic calcium phosphate preparations. Calcif Tissue Res 1972;10:171–197.
39. Eanes ED, Termine JD, Nylen MU. Electron microscopic study of the formation of amorphous calcium phosphate and its transformation to crystalline apatite. Calcif Tissue Res 1973;12:143–158.
40. Greenfield DJ, Termine JD, Eanes ED. Chemical study of apatites prepared by hydrolysis of amorphous calcium phosphates in carbonate-containing aqueous solutions. Calcif Tissue Res 1974;14:131–138.
41. Eanes ED. The interaction of supersaturated calcium phosphate solutions with apatitic substrates. Calcif Tissue Res 1976;20:75–89.
42. Eanes ED, Meyer JL. The maturation of crystalline calcium phosphates in aqueous solutions at physiologic pH. Calcif Tissue Res 1977;23:259–269.
43. Skrtic D, Antonucci JM, Eanes ED, Eidelman N. Dental composites based on hybrid and surface-modified amorphous calcium phosphates. Biomaterials 2004;25:1141–1150.
44. Rey C, Beshah K, Griffin R, Glimcher MJ. Structural studies of the mineral phase of calcifying cartilage. J Bone Miner Res 1991;6:515–525.
45. Wu YT, Glimcher MJ, Rey C, Ackerman JL. A unique protonated phosphate group in bone-mineral not present in synthetic calcium phosphates—Identification by P-31 solid-state NMR spectroscopy. J Mol Biol 1994;244:423–435.
46. Rey C, Hina A, Tofighi A, Glimcher MJ. Maturation of poorly crystalline apatites: Chemical and structural aspects in vivo and in vitro. Cells Mater 1995;5:345–356.
47. Quizat S, Barroug A, Legrouri A, Rey C. Adsorption of bovine serum albumin on poorly crystalline apatite: Influence of maturation. Mater Res Bull 1999;34:2279–2289.
48. Tofighi A, Mounic S, Chakravarthy P, Rey C, Lee D. Setting reactions involved in injectable cements based on amorphous calcium phosphate. Key Eng Mater 2000;192–1:769–772.
49. Benaziz L, Barroug A, Legrouri A, Rey C, Lebugle A. Adsorption of *o*-phospho-L-serine and L-serine onto poorly crystalline apatite. J Colloid Interf Sci 2001;238:48–53.
50. Kim HM, Kim YS, Woo KM, Park SJ, Rey C, Kim Y, Kim JK, Ko JS. Dissolution of poorly crystalline apatite crystals by osteoclasts determined on artificial thin-film apatite. J Biomed Mater Res 2001;56:250–256.
51. Somrani S, Rey C, Jemal M. Thermal evolution of amorphous tricalcium phosphate. J Mater Chem 2003;13:888–892.
52. Cazalbou S, Combes C, Eichert D, Rey C, Glimcher MJ. Poorly crystalline apatites: Evolution and maturation in vitro and in vivo. J Bone Miner Metab 2004;22:310–317.

53. Knabe C, Berger G, Gildenhaar R, Howlett CR, Markovic B, Zreiqat H. The functional expression of human bone-derived cells grown on rapidly resorbable calcium phosphate ceramics. Biomaterials 2004;25:335–344.
54. Ramselaar MMA, Driessens FCM, Kalk W, de Wijn JR, van Mullem PJ. Biodegradation of four calcium phosphate ceramics; in vivo rates and tissue interactions. J Mater Sci: Mater Med 1991;2:63–70.
55. Driessens FCM, Ramselaar MMA, Schaeken HG, Stols ALH, van Mullem PJ. Chemical reactions of calcium phosphate implants after implantation in vivo. J Mater Sci: Mater Med 1992;3:413–417.
56. Ramselaar MMA, van Mullem PJ, Kalk W, de Wijn JR, Stols ALH, Driessens FCM. In vivo reactions to particulate rhenanite and particulate hydroxylapatite after implantation in tooth sockets. J Mater Sci: Mater Med 1993;4:311–317.
57. Bermudez O, Boltong MG, Driessens FCM, Ginebra MP, Fernandez E, Planell JA. Chloride- and alkali-containing calcium phosphates as basic materials to prepare calcium phosphate cements. Biomaterials 1994;15:1019–1023.
58. Knabe C, Gildenhaar R, Berger G, Ostapowicz W, Fitzner R, Radlanski RJ, Gross U. Morphological evaluation of osteoblasts cultured on different calcium phosphate ceramics. Biomaterials 1997;18:1339–1347.
59. Suchanek W, Yashima M, Kakihana M, Yoshimura M. β-rhenanite (β-NaCaPO$_4$) as weak interphase for hydroxyapatite ceramics. J Eur Ceram Soc 1998;18:1923–1929.
60. Gong W, Abdelouas A, Lutze W. Porous bioactive glass and glass-ceramics made by reaction sintering under pressure. J Biomed Mater Res 2001;54:320–327.
61. El-Ghannam AR. Advanced bioceramic composite for bone tissue engineering: Design principles and structure–bioactivity relationship. J Biomed Mater Res A 2004;69:490–501.
62. Apel E, Holand W, Rheinberger V. Bioactive rhenanite glass ceramic. US Pat. Appl. No. 2004/0167006 A1.
63. Glasser FP, Gunawardane RP. Fertilizer material from apatite. US Pat. No. 4,363,650, December 14, 1982.
64. OsteoStim® resorbable bone graft substitute. EBI L.P., Parsippany, NJ, 2006. Available at: www.ebimedical.com/products.
65. Eppley B, Stal S, Hollier L, Kumar M. Compartmentalized bone regeneration of cranial defects with biodegradable barriers—Effects of calcium sodium phosphate surface coatings on LactoSorb. J Craniofac Surg 2002;13:681–686.
66. Biomet, Inc. Calcigen™-NaP bone void filler. Biomet, Inc., Warsaw, IN, 2006.
67. Tas AC. Synthesis of biomimetic Ca-hydroxyapatite powders at 37°C in synthetic body fluids. Biomaterials 2000;21:1429–1438.
68. Lee DD, Rey C, Aiolova M, Tofighi A. Bioresorbable ceramic composites. US Pat. No. 6,331,312, December 18, 2001.
69. Hiller JC, Thompson TJU, Evison MP, Chamberlain AT, Wess TJ. Bone mineral change during experimental heating: An X-ray scattering investigation. Biomaterials 2003;24:5091–5097.
70. Rogers KD, Daniels P. An X-ray diffraction study of the effects of heat treatment on bone mineral microstructure. Biomaterials 2002;23:2577–2585.
71. Spoerke ED, Stupp SI. Synthesis of a poly(L-lysine)-calcium phosphate hybrid on titanium surfaces for enhanced bioactivity. Biomaterials 2005;26:5120–5129.
72. Tas AC, Bhaduri SB. Chemical processing of CaHPO$_4$ 2H$_2$O: Its conversion to hydroxyapatite. J Am Ceram Soc 2004;87:2195–2200.
73. Tas AC, Majewski PJ, Aldinger F. Chemical preparation of pure and strontium- and/or magnesium-doped lanthanum gallate powders. J Am Ceram Soc 2000;83:2954–2960.
74. Tas AC. Combustion synthesis of calcium phosphate bioceramic powders. J Eur Ceram Soc 2000;20:2389–2394.
75. ICDD PDF No. 29–1193. The International Centre for Diffraction Data. Newtown Square, PA.
76. Doi Y, Shimizu Y, Moriwaki Y, Aga M, Iwanaga H, Shibutani T, Yamamoto K, Iwayama Y. Development of a new calcium phosphate cement that contains sodium calcium phosphate. Biomaterials 2001;22:847–854.
77. Pleshka N, Boskey A, Mendelsohn R. Novel infrared spectroscopic method or determination of crystallinity of hydroxyapatite minerals. Biophys J 1991;60:786–793.
78. Madsen HEL, Thodvadarson G. Precipitation of calcium phosphate from moderately acid solutions. J Cryst Growth 1984;66:369–376.
79. Inskeep WP, Silvertooth JC. Kinetics of hydroxyapatite precipitation at pH 7.4 to 8.4. Geochim Chosmochim Acta 1988;52:1883–1893.
80. Ebrahimpour E, Johnson M, Richardson CF, Nancollas GH. The characterization of HA precipitation. J Colloid Interface Sci 1993;159:158–163.
81. Zhou J, Zhang X, Chen J, Zeng S, de Groot K. High temperature characteristics of synthetic hydroxyapatite. J Mater Sci: Mater Med 1993;4:83–85.
82. LeGeros RZ, LeGeros JP. Dense hydroxyapatite. In: Hench LL, Wilson J, editors. An Introduction to Bioceramics. London: World Scientific; 1993. pp 144, 145.
83. Loong CK, Rey C, Kuhn LT, Combes C, Wu Y, Chen SH, Glimcher MJ. Evidence of hydroxyl-ion deficiency in bone apatites: An inelastic neutron-scattering study. Bone 2000;26:599–602.
84. Rey C, Shimizu M, Collins B, Glimcher MJ. Resolution-enhanced Fourier transform infrared spectroscopy study of the environment of phosphate ion in the early deposits of a solid phase of calcium phosphate in bone and enamel and their evolution with age: 2. Investigations in the ν_3 PO$_4$ domain. Calcif Tissue Int 1991;49:383–388.
85. Lin SY, Chen KH, Li MJ, Cheng WT, Wang SL. Evidence of octacalcium phosphate and type-B carbonated apatites deposited on the surface of explanted acrylic hydrogel intraocular lens. J Biomed Mater Res B Appl Biomater 2004;70:203–208.
86. Robinson RA, Watson ML. Collagen-crystal relationships in bone as seen in the electron microscope. Anat Rec 1952;114:383–410.
87. Johansen E, Parks HF. Electron microscopic observations on the three-dimensional morphology of apatite crystallites of human dentine and bone. J Biophys Biochem Cytol 1960;7:743–746.
88. Molnar Z. Additional observations on bone crystal dimensions. Clin Orthop 1960;17:38–42.
89. Molnar Z. Development of the parietal bone of young mice. I. Crystals of bone mineral in frozen-dried preparations. J Ultrastruct Res 1959;3:39–45.
90. Posner AS, Eanes ED, Harper RA, Zipkin I. X-ray diffraction analysis of the effect of fluoride on human bone apatite. Arch Oral Biol 1963;8:549–570.
91. Nakahira A, Konishi S, Nishimura F, Iwasaka M, Ueno S. Effect of a high magnetic field on the bioactivity of apatite-based biomaterials. J Appl Phys 2003;93:8513–8515.
92. Hata K, Kokubo T, Nakamura T, Yamamuro T. Growth of a bonelike apatite layer on a substrate by a biomimetic process. J Am Ceram Soc 1995;78:1049–1053.
93. Bayraktar D, Tas AC. Chemical preparation of carbonated calcium hydroxyapatite powders at 37°C in urea-containing synthetic body fluids. J Eur Ceram Soc 1999;19:2573–2579.
94. Doi Y, Koda T, Wakamatsu N, Goto T, Kamemizu H, Moriwaki Y, Adachi M, Suwa Y. Influence of carbonate on sintering of apatites. J Dent Res 1993;72:1279–1284.
95. Tas AC, Bhaduri SB. Rapid coating of Ti6Al4V at room temperature with a calcium phosphate solution similar to 10x simulated body fluid. J Mater Res 2004;19:2742–2749.

96. Kivrak N, Tas AC. Synthesis of calcium hydroxyapatite-tricalcium phosphate (HA-TCP) composite bioceramic powders and their sintering behavior. J Am Ceram Soc 1998;81:2245–2252.
97. Kangasniemi IMO, de Groot K, Becht JGM, Yli-Urpo AU. Preparation of dense hydroxylapatite or rhenanite containing bioactive glass composites. J Biomed Mater Res 1992;26:663–674.
98. Kangasniemi IMO, Vedel E, de Blick-Hogerworst J, Yli-Urpo AU, de Groot K. Dissolution and scanning electron microscopic studies of Ca, P particle-containing bioactive glasses. J Biomed Mater Res 1993;27:1225–1233.
99. Yuan H, van Den Doel M, Li S, van Blitterswijk CA, de Groot K, de Bruijn JD. A comparison of the osteoinductive potential of two calcium phosphate ceramics implanted intramuscularly in goats. J Mater Sci: Mater Med 2002;13:1271–1275.
100. Kurashina K, Kurita H, Wu Q, Ohtsuka A, Kobayashi H. Ectopic osteogenesis with biphasic ceramics of hydroxyapatite and tricalcium phosphate in rabbits. Biomaterials 2002;23:407–412.
101. Le Nihouannen D, Daculsi G, Saffarzadeh A, Gauthier O, Delplace S, Pilet P, Layrolle P. Ectopic bone formation by microporous calcium phosphate ceramic particles in sheep muscles. Bone 2005;36:1086–1093.